

Size-dependent magnetic properties of Nickel nano-chains

Wangzhi Zheng, Chinpings Chen^(a), Lin He

Department of Physics, Peking University, Beijing, 100084, China

Wei Zhou, Chenmin Liu, Lin Guo^(b), Huibin Xu

School of Materials Science and Engineering, Beijing University of Aeronautics and Astronautics, Beijing, 100083, China

PACS : 75.75.+a, 81.07.-b

ABSTRACT

Various sizes of Ni nano-chains, including 50 nm, 75 nm, and 150 nm, have been synthesized by a wet chemical route. The characterizations by XRD and TEM indicate that the samples are consisting of pure Ni polycrystalline nano-particles, with light carbon encapsulation, forming one dimensional (1D) chain-like structure. Double anisotropic behaviors are observed by the field-cooled (FC) and zero-field-cooled (ZFC) measurements. One is in the low temperature region, resulting from the amorphous or anisotropic surface magnetism of the nano-particles. The other has exhibited anisotropic energy higher than room temperature, owing to the shape anisotropy of 1D geometry. A magnetic core-shell structure can reasonably explain the surface magnetism and the 1D anisotropy resulting from the core magnetism. The surface magnetism is significantly enhanced at low temperature, becoming more pronounced with the decreasing size. The effect of 1D anisotropy, in particular, is probed in detail by the ZFC measurements on the 50 nm samples under various measuring fields. Magnetic nano-domain size in the core phase is estimated roughly as 11 nm, smaller than the particle size of the sample.

INTRODUCTION

In recent years, nano-scaled magnetic materials have received much attention, due to the fundamental interest in the unique magnetic property different from that in the bulk phase and to their promising applications in technology such as in the high-density magnetic storage, etc. The magnetic properties are usually dictated by the size, dimension, shape, structure, morphology of the constituent phases, along with the type and strength of magnetic coupling between them. The magnetic metals, including Fe, Co, Ni, and their related compounds or alloys in low dimensional form, are one of the most important subjects to study. Many of the nano-objects with these materials in various shapes have already been fabricated or synthesized by different techniques [1-7]. Investigations into some of the interesting magnetic properties have been conducted as well [8]. With the nano-particles, the properties under intensive study include the disorder state of surface spin and the related blocking behavior, the magnetic dynamics, the surface anisotropy, the magnetization reversal, the dipolar interaction effect, the superparamagnetic property, etc., [9-13]. In the meanwhile, with the one dimensional (1D) nano-objects, such as the nanorods [2,14], or nanowires [15-17], the investigations are concentrated more or less on the magnetization reversal and effect of shape anisotropy.

The surface effect associated with the magnetic nano-particles often shows complicated properties, especially under interaction with the surrounding particles. Some experiments have reported that the moment reduces with the decreasing size [18,19], while others, obtained the same value as that in the bulk phase [20]. By contrast, experiment performed on the Fe, Co, and Ni clusters has demonstrated that the magnetic moment is atom-like with the cluster size less than 30 atoms. It decreases, approaching the bulk limit as the particle size increases to 700 atoms or so [21]. Very recently, pure Ni nanochains have been synthesized for the first time by a technique of wet chemical solution [22]. It provides a unique model system for the fundamental investigation into the magnetism associated with the surface spin state of

nano-particles along with the shape anisotropy from the 1D structure. In this paper, the magnetism in Ni nano-chains, with sizes ranging from 50 nm to 150 nm, have been under extensive study. The thermal behavior of the magnetization, by the field-cooled (FC) and zero-field-cooled (ZFC) measurements, has exhibited features related to the freezing of amorphous spin state on the sample surface at low temperature and to the trapping of the magnetic moment in the anisotropic potential attributed to the 1D shape anisotropy of the chain-like structure.

SAMPLE PREPARATION AND CHARACTERIZATION

Synthesis of the sample has been made by the technique of wet chemical solution, the same as our previous report[22]. The chain-like structure is formed by a self-assembled process of the Ni nano-particles with the modification of the PVP. Three different sizes are obtained, including 50 nm, 75 nm, and 150 nm, with a size distribution of about 10 nm, labeled as S50, S75 and S150, respectively. The samples have a typical length of a few micrometers. Typical SEM images of the S50, S75 and S150 samples are shown in Fig. 1. In Fig. 1a, the residual PVP is vaguely visible surrounding the Ni chain. The averaged particle size is about 50 nm in Fig. 1a, 75 nm in Fig. 1b and 150 nm in Fig. 1c. The particles are structurally connected together, forming chain-like networks. In particular, the ones in Fig. 1c have almost grown into wires.

Figure 2 shows XRD patterns of the products. The ones with 50 nm, by curve (a), and 75 nm, by (b), are similar. The main peaks marked with stars correspond to the face centered cubic (fcc) nickel (JCPDS 04-0850), while the remaining weak peaks conform to the crystal planes of nickel carbide with the trigonal system (JCPDS77-0194). The surface carbonization of the nickel nano-chains as the diameter less than 75 nm may lead to the existence of the nickel carbide on the surface of the pure Ni determined by XRD. Comparing to (a) and (b), the peaks appearing in curve (c) can easily be indexed as pure fcc nickel (JCPDS 04-0850).

MEASUREMENTS AND ANALYSIS

The magnetic measurements on the powdered sample have been performed using SQUID magnetometer (Quantum Design). The ZFC/FC magnetizations are recorded at the applied field, $H_{\text{app}} = 90$ Oe, while warming up from 5 K. In the cooling leg for the FC measurement, the field is 2 Tesla. For all the three samples, the two branches of FC/ZFC curves separate from each other with the temperature going up to 395 K, as shown in Fig. 3a. It evidences a ferromagnetic ordering with a potential barrier separating the easy axis from the axis of the applied field. The shape anisotropy is obvious with the 1D chain-like structure of the sample. With the FC measurement, the magnetic moment is aligned along the orientation of the applied field during the cooling process and, then, frozen at low temperature due to the anisotropic potential. As the temperature is going up after the cooling field is ramped off, the magnetization, M_{FC} , is reducing. This is attributed to the thermal activation effect reorienting the magnetic moment to the orientation of the easy axis, which differs from the applied field. On the other hand, with the ZFC, the magnetic moment tends to be frozen, pointing along the easy axis of each individual nano-chain, which is randomly oriented in every direction. At the increasing temperature during the measurement under the small field of 90 Oe, M_{ZFC} increases as the magnetic moment is thermally activated, aligned more or less along the field direction. The magnitude of the FC magnetization, M_{FC} , shows significant size effect, going down with the reducing size. It indicates that the magnetism is coming from the core of the samples, rather than from the surface layer. On the other hand, the ZFC curves in the low temperature region exhibit a peak structure at about 13 K, see Fig. 3b. There is no obvious dependence of the peak positions on the sample size. The peak height, however, increases with the reducing sample size, suggesting that the contribution is from the surface magnetism.

The ZFC data for S50 recorded at 90 Oe, 200 Oe, 500 Oe, 800 Oe, and 1 kOe, along with a FC curve measured at 1 kOe, are plotted in Fig. 4a. As the applied field

for the measurement increases, a softening-like downward trend becomes more obvious in the high temperature region. Eventually, the ZFC and FC curves collapse at the applied field of 1 kOe, except in the low temperature region where the ZFC/FC curves exhibit a typical blocking feature. This evidences that the peak in the M_{ZFC} at low temperature is a feature of the freezing behavior, owing to the surface amorphous spin state or surface anisotropy. The peak position shifts down slightly, about 1 K, with the progressively increasing applied field of measurement, see the inset of Fig. 4a, further confirming the freezing property. On the other hand, the softening feature in the high temperature region is a sign that the thermal energy is comparable with the 1D shape anisotropic energy in the presence of applied field. More interesting ZFC property is revealed in the plot of the susceptibility, $\chi(H) = M_{ZFC}(H)/H$, versus temperature, presented in Fig. 4b. At $T < 260$ K, the curves of susceptibility recorded at 90 Oe and 200 Oe almost coincide with each other, going up linearly with the temperature. However, the data recorded at 200 Oe has shown a softening feature. It departs from the linearity at 260 K. While, the linearity for the 90 Oe data persists to the high temperature limit of measurement at 395 K, see Fig.4b. This indicates that, for the moment initially trapped in the anisotropic potential, the thermal activation energy has become comparable to the anisotropic energy under the applied field. With the field increasing to 500 Oe, the temperature at which the susceptibility deviates from the linearity drops to about 115 K. As the field further increases to 800 Oe and 1 kOe, the field effect on the magnetic moment would dominate the anisotropic energy and the thermal activation. Note that the sample has been kept in room temperature for a few days before every run, so that the magnetism can relax to ensure a reliable ZFC measurement.

The field dependent magnetization (M-H) measurements at 5 K, 300 K, and 380 K, on S50 are plotted in Fig. 5, showing open hysteresis loops. For the M-H data taken at 5 K, which is below the blocking temperature, $T_b \sim 13$ K, the loop is much more pronounced in comparison with the ones measured at high temperatures. This indicates the important contribution from the surface magnetism. The saturation

magnetization determined in the high field region ~ 5 Tesla, see the inset, are 25 emu/g (5 K), 11.0 emu/g (300 K), and 10.8 emu/g (380 K), corresponding to the effective moment of $0.263 \mu_B$, $0.116 \mu_B$, and $0.113 \mu_B$ per Ni atom, respectively. This is smaller than the listed bulk value of $0.606 \mu_B$ per Ni atom at 300 K. The much enhanced moment obtained at $T < T_b$ suggests that the surface magnetism is indeed very important for the nano-sized particles, in consistent with the results in the ZFC/FC measurements. The field dependent measurements have been carried out for S75 and S150 as well. The saturation magnetizations, coercivities are summarized in Tab. 1. The saturation magnetization is larger for the large size sample. For S150 at 300 K, the value is 46 emu/g, reaching 80% of the bulk limit. This suggests that the magnetism start deviating from the bulk value at the size around 150 nm or so. On the other hand, the coercivity reduces with the decreasing sample size. In Fig 6, the coercivity field, H_C , determined from the loops in Fig. 5 is plotted along with $\Delta M = M_{FC} - M_{ZFC}$ on the temperature scale for S50. These two exhibit a proportional relation, showing a further indication on the important contribution of the surface magnetism to the hysteresis loop.

DISCUSSION

The isothermal time relaxation of the ZFC magnetization for S50 has been measured at 5 K, 50 K and 100 K with the recording field of 200 Oe. Using the simple equation, $M(t) = M_1 + M_2(1 - e^{-t/\tau})$, to approximate the relaxation behavior, then, M_2/M_{ZFC} accounts for only 5 % at 5 K, 1.2 % at 50 K, and 2 % at 100 K, with the measuring time of two hours. Hence, the FC/ZFC data presented is a reasonable approximation to the equilibrium value. On the other hand, the magnetism of Ni_3C phase and the effect of the carbon encapsulation on the magnetism of Ni has been investigated previously[23,24]. The results indicated that the nickel carbide is expected not to have ferromagnetism and the magnetism of Ni is not modified profoundly in the presence of the Ni_3C phase. The magnetic properties of the Ni phase are, therefore, not affected in the presence of little nickel carbide phase detected in the

XRD patterns, Fig. 2.

The results of ZFC/FC and M-H measurements can be reasonably explained by the magnetic core-shell structure [19]. The surface amorphous spin state or anisotropy has led to the typical freezing behavior at low temperature in the FC/ZFC curves, causing the peak-like structure at about 13 K in the ZFC measurement. On the other hand, the high temperature anisotropy is owing to the moment from the core having the 1D anisotropic coupling, which is stronger than the dipolar nature owing to the chain-like structure. In the field dependent measurement, the saturation magnetizations and the hysteresis loops are dramatically enhanced at $T = 5 \text{ K} < T_b$, as shown in Fig. 5 for S50 sample as well as for the other samples not shown. This directly demonstrates the excessive contributions to the magnetism from the surface layer and evidences that the enhanced open hysteresis, at $T < T_b$, is partly due to the transition between the surface spin configurations.

In Fig. 3, the M_{ZFC} for S50 is recorded at various fields, demonstrating the competing effect of the magnetic energy, $E_{\text{mag}} = \mu_{\text{FM}}H$, and the thermal energy, $k_B T$, in the presence of 1D anisotropic energy, E_a . At the point where the susceptibility, in Fig. 4, deviates from the linear relation with the temperature, the thermal activation effect begins taking over as the leading energy factor on the magnetic moment in the core. This characteristic temperature can be described by the simple relation, $(E_a - E_{\text{mag}}) \sim k_B T$. With the assumption that $\mu_{\text{FM}} \sim N\mu_B$ is the averaged magnitude of the ferromagnetic moment participating in the magnetization reversal under the effect of applied field or thermal activation, one can estimate that $N \sim 7200$ by the two characteristic temperatures of deviation, 260 K and 115 K corresponding to the curves with 200 Oe and 500 Oe in Fig. 4. Using the effective moment, $0.11 \mu_B/\text{Ni-atom}$, obtained in the saturation region at 300 K, the number of Ni atoms forming a single magnetic domain in the core is then estimated as 65000, which is equal to the domain size $D \sim 11 \text{ nm}$. Hence, for the S50 sample, each Ni nano-particle contains about 10 to 20 such magnetic nano-domains. On the other hand, the thickness of the magnetic

shell phase is estimated as about 5 nm with the S150 sample, under the assumption that the saturation magnetization at 300 K in the core phase is equal to the bulk value and the contribution from the shell phase is negligible. The exchange length, which characterizing the spatial range of exchange-coupled region, is 8 nm and 47 nm with Ni for the perpendicular and parallel components, respectively [25]. Therefore, with the chain-like structure of the present sample, the exchange coupling prevail against the magnetostatic field between the adjacent nano-particles, considering that the shell thickness estimated in the above does not exceed the characteristic exchange lengths.

CONCLUSION

We have performed magnetic measurements on the Ni nano-chains with sizes of 50 nm, 75 nm, and 150 nm. The magnetic properties can be explained reasonably by the core-shell model. The sample exhibits enhanced magnetism at low temperature arising from the surface spin-glass state or surface anisotropy. At $T < T_b$, the effective moment obtained in the saturation increases dramatically from the value at high temperature. It suggests that the enhanced open hysteresis, at $T < T_b$, is partly due to the transition between surface spin configurations, on top of the contribution from the magnetization reversal in the core. The averaged magnetic moment is shown to reduce with the decreasing sample size. However, the magnetism associated with the surface phase becomes pronounced as the particle size goes down, as expected from many previous results on magnetic nano-particles. On the other hand, the 1D shape anisotropy is probed, in particular, by the ZFC measurement on the S50 sample with various measuring fields. The size of the magnetic nano-domain in the core phase is estimated as $D \sim 11$ nm with the S50 sample, and the shell thickness, ~ 5 nm, with the S150 sample. The present experiment is the first one to report in detail the interesting magnetic properties of Ni nano-chains, showing both the freezing property of surface spins and the 1D anisotropic magnetism in the core.

Acknowledgement

This project is financially supported by National Natural Science Foundation of China (20373004) and the Program for New Century Excellent Talents in University (NCET) as well as by Engineering Research Institute, Peaking University (ERIPKU).

References

a) e-mail: cpchen@pku.edu.cn

b) e-mail: guolin@buaa.edu.cn

[1] V.F. Puentes, K.M. Krishnan, and A.P. Alivisatos, *Science* **291**, 2115 (2001)

[2] S.W. Jung, W.I. Park, G.-C. Yi, M.Y. Kim, *Adv. Mater.* **15**, 1358 (2003)

[3] J.C. Bao, Y.Y. Liang, Z. Xu, L. Si, *Adv. Mater.* **15**, 1832 (2003)

[4] L.T. Yu, I.A. Banerjee, M. Shima, K. Rajan, and H. Matsui, *Adv. Mater.* **16**, 709 (2004)

[5] L. Guo, C.M. Liu, R.M. Wang, H.B. Xu, Z.Y. Wu, and S.H. Yang, *J. Am. Chem. Soc.* **126**, 4530 (2004)

[6] R.M. Wang, C.M. Liu, H.Z. Zhang, C.P. Chen, L. Guo, H.B. Xu, and S.H. Yang
Appl. Phys. Lett. **85**, 2080 (2004)

[7] L. Guo, C.M. Liu, R.M. Wang, H.B. Xu, Z.Y. Wu, and S.H. Yang, *J. Am. Chem. Soc.*, **126**, 4530 (2004)

[8] R. Skomski, *J. Phys. Condens. Matter* **15**, R841 (2003)

[9] R.H. Kodama, A.E. Berkowitz, E.J. McNiff, Jr. and S. Foner, *Phys. Rev. Lett.* **77**, 394 (1996)

[10] B. Martínez, X. Obradors, Ll. Balcells, A. Rouanet, C. Monty, *Phys. Rev. Lett.*

80, 181 (1998)

- [11] G. F. Goya, F. C. Fonseca, R. F. Jardim, R. Muccillo, N. L. V. Carreno, E. Longo, E. R. Leite, J. App. Phys. **93**, 10 (2003)
- [12] S. Sahoo, O. Petracia, W. Kleemann, S. Stappert, G. Dumpich, P. Nordblad, S. Cardoso, and P. Freitas, Appl. Phys. Lett. **82**, 4116 (2003)
- [13] E. Bonetti, L. D. Bianco, D. Fiorani, D. Rinaldi, R. Caciuffo, A. Hernando, Phys. Rev. Lett. **83**, 2829 (1999)
- [14] N. Cordente, M. Respaud, F. Senocq, M.-J. Casanove, C. Amiens, and B. Chaudret, Nano Lett. **1**, 565 (2001)
- [15] B. Leven, G. Dumpich, Phys. Rev. B **71**, 064411 (2005)
- [16] M. Zhang, L. Menon, H. Zeng, Y. Lin, S. Bandyopadhyay, R.D. Kirby, and D.J. Sellmyer, Phys. Rev. B **62**, 12282 (2000)
- [17] R. Skomski, H. Zeng, M. Zheng, and D.J. Sellmyer, Phys. Rev. B **62**, 3900 (2000)
- [18] F. Luis, J.M. Torres, L.M. Garcí'a, J. Bartolome', J. Stankiewicz, F. Petroff, F. Fettar, J.-L. Maurice, and A. Vaures, Phys. Rev. B **65**, 094409 (2002)
- [19] R.H. Kodama, A.E. Berkowitz, E.J. McNiff, Jr., and S. Foner, Phys. Rev. Lett. **77**, 394 (1996)
- [20] Y.R. Uhm, J.H. Park, W.W. Kim, C.-H. Cho, C.K. Rhee, Mater. Sci. Eng. B **106**, 224 (2004)
- [21] I.M.L. Billas, A. Chatelain, and W.A. de Heer, Science **265**, 1682 (1994)
- [22] C.M. Liu, L. Guo, R.M. Wang, Y. Deng, H.B. Xu, and S.H. Yang, Chem. Comm.

2726 (2004)

- [23] L.P. Yue, R. Sabiryanov, E.M. Kirkpatrick, and D.L. Leslie-Pelecky, Phys. Rev. B **62**, 8969 (2000)
- [24] X.-C. Sun, X.-L. Dong, Mater. Res. Bull. **37**, 991 (2002)
- [25] R.C. O'Handley, P296 in "Modern Magnetic Materials Principles and Applications (John Wiley & Sons, New York, 2000)

FIGURES

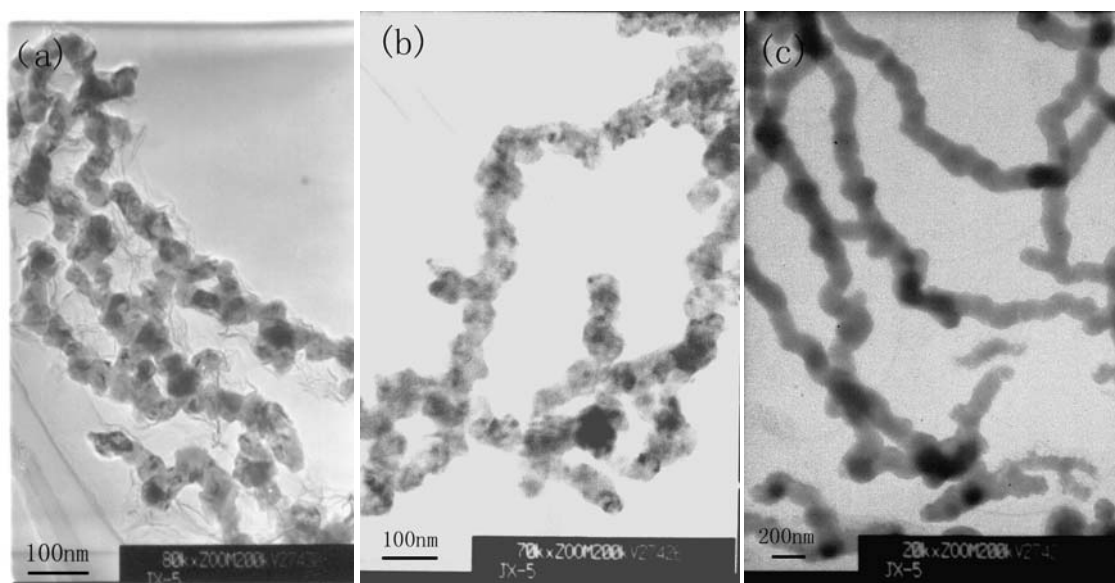


Fig. 1 TEM images of the nano-chains. (a) ~ 50 nm nickel chains capped with residual PVP. (b) ~ 75 nm nickel chains with uniform structure. (c) chains with the size of 150 nm.

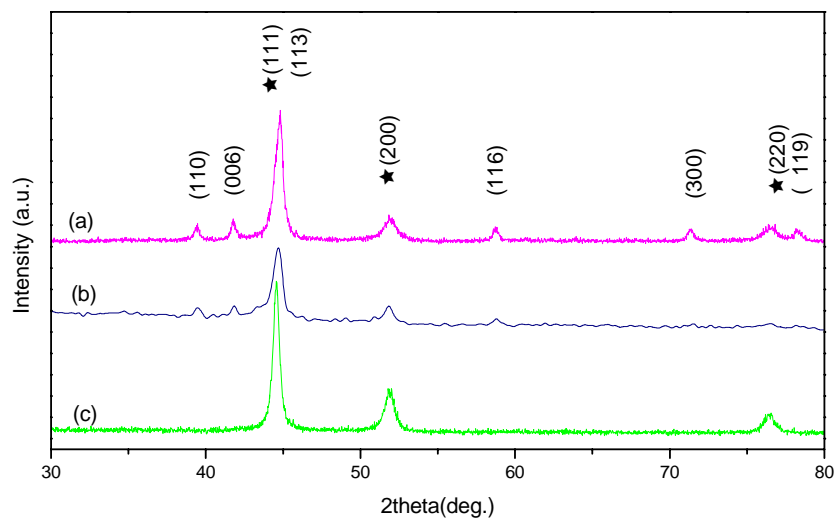


Fig. 2 XRD patterns with various sizes. (a) pure nickel of 50 nm capped with nickel carbide. (b) pure nickel of 75 nm with nickel carbide. (c) pure nickel nano-chains of 150 nm.

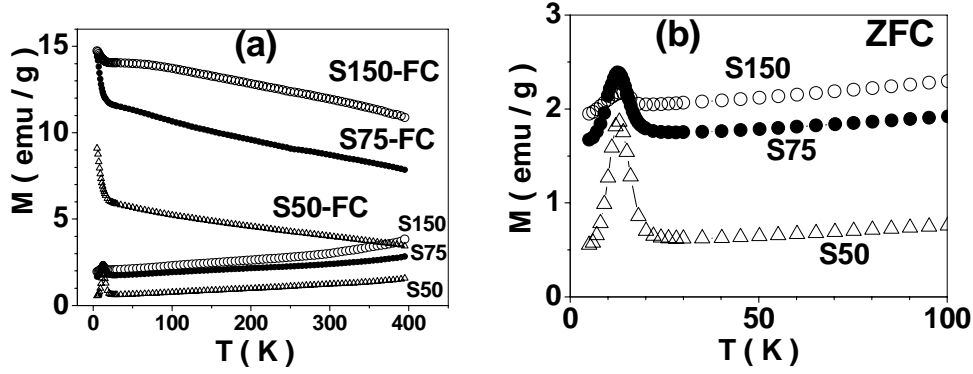


Fig. 3 FC/ZFC measurements recorded at $H_{app} = 90$ Oe. (a) The measurement is from 5 K to 395 K. For the FC measurement, the field in the cooling process is 2 Tesla. (b) M_{ZFC} in the low temperature region is shown to better reveal the peaks around 13 K. The peak position does not depend on the size, while, the peak height clearly exhibits size effect. The smaller the sample size, the larger the peak height.

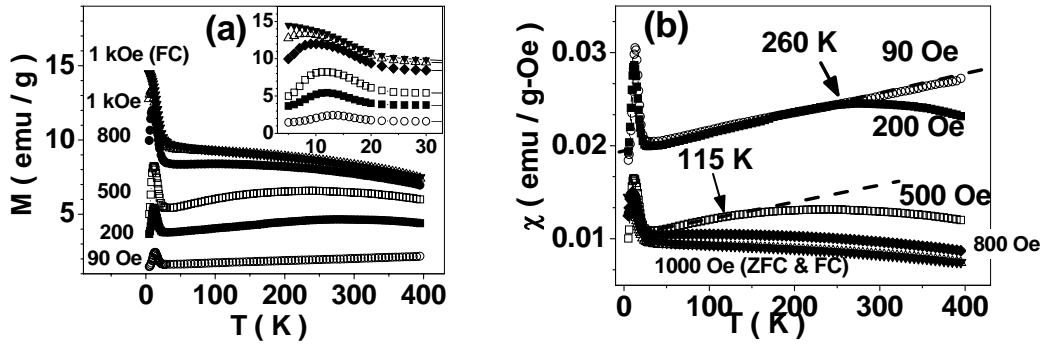


Fig. 4 M - T and χ - T for S50 sample. (a) ZFC M - T data recorded at the applied field of 90 Oe, 200 Oe, 500 Oe, 800 Oe, and 1 kOe. The FC curve measured at 1 kOe is included. The inset shows the data in the low temperature region. The FC/ZFC curves recorded at 1 kOe exhibit a typical blocking behavior at about 10 K, merging together. (b) The susceptibility, $\chi = M/H$, calculated from the M - T data in (a). The two parallel dash lines are drawn to show the linear temperature behavior of χ at low measurement field.

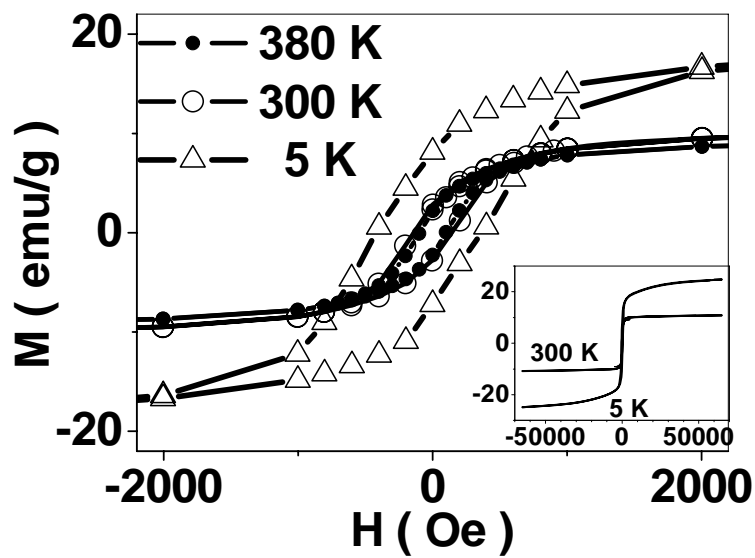


Fig. 5 Hysteresis loops measured at 5 K, 300 K, 380 K. The inset gives the results to the saturation region.

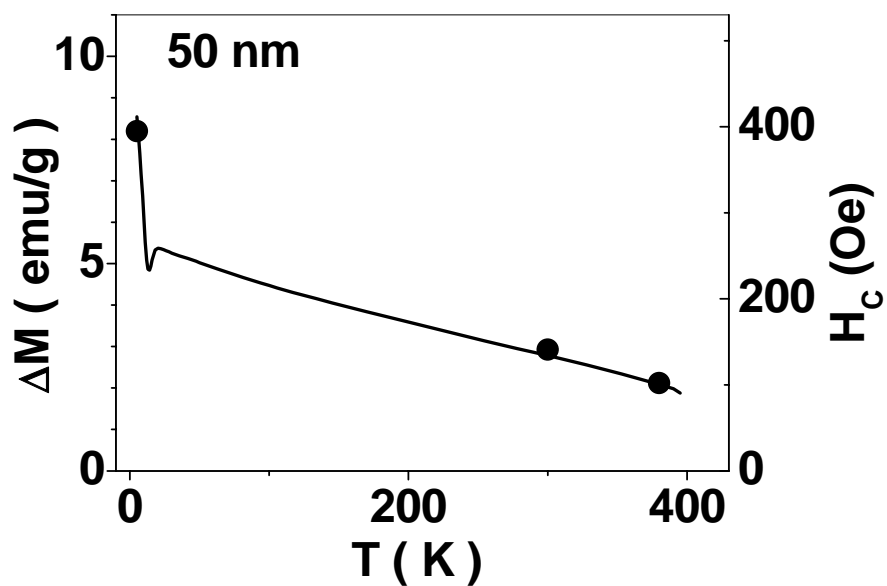


Fig.6 Difference in the magnetization between ZFC and FC measurement, $\Delta M = M_{FC} - M_{ZFC}$, under the applied field of 90 Oe. The inset shows the data in the low temperature region.

	M _S (300K)		M _S (5K)		H _C (Oe) 300 K	H _C (Oe) 5 K
	emu/g	μ _B /Ni	emu/g	μ _B /Ni		
50 nm	11	0.12	25	0.26	139	392
75 nm	33	0.35	44	0.46	124	305
150 nm	46	0.48	552	0.55	102	195

Table 1 Saturated magnetizations and coercivities for S50, S75 and S150 at 5 K and 300 K.